Tailoring Plasmonic and Electrostatic Field Effects To Maximize Solar Energy Conversion by Bacteriorhodopsin, the Other Natural Photosynthetic System

ARTICLE *in* NANO LETTERS · AUGUST 2011

Impact Factor: 13.59 · DOI: 10.1021/nl2018959 · Source: PubMed

5 AUTHORS, INCLUDING:

Steven C Hayden
Aramco Research Center, Cambridge MA, USA
14 PUBLICATIONS **212** CITATIONS
SEE PROFILE

Erik Christopher Dreaden
Massachusetts Institute of Technology
32 PUBLICATIONS **1,907** CITATIONS
SEE PROFILE

Mostafa A El-Sayed
Georgia Institute of Technology
675 PUBLICATIONS **54,634** CITATIONS
SEE PROFILE

NANO LETTERS

LETTER

pubs.acs.org/NanoLett

Tailoring Plasmonic and Electrostatic Field Effects To Maximize Solar Energy Conversion by Bacteriorhodopsin, the Other Natural Photosynthetic System

Chun-Wan Yen,[†] Steven C. Hayden,[†] Erik C. Dreaden, Paul Szymanski, and Mostafa A. El-Sayed*

Laser Dynamics Laboratory, School of Chemistry and Biochemistry, Georgia Institute of Technology, Atlanta, Georgia 30332-0400, United States

Supporting Information

ABSTRACT: We have explored the plasmonic field enhancement of current production from bacteriorhodopsin (bR) by maximizing the blue light effect, where the influx of blue photons absorbed by the long-lived M intermediate drastically shortens the time scale of the bR photocycle, leading to current enhancement. To this end, we used three approaches in our solution-based cell: (1) We improved the charge carrier separation in solution through the use of a proton-selective Nafion membrane. (2) We maximized the plasmonic surface field effects by selecting the capping polymer with minimum surface field screening and best nanoparticle stability. (3) We selected the plasmonic nanoparticle with the strongest plasmonic field whose surface plasmon resonance has the largest spectral overlap with the blue light absorbing M-intermediate. Theoretical models are used to explain experimental results, which show a 40 nm cuboidal nanoparticle capped with 55k PVP polymer to give the best photocurrent enhancement. Enhanced by this particle, bR in our Nafion membrane solution cell gave a photocurrent of 0.21 μA/cm^3, which is 5000 times larger than the published results for thin film bR electrochemical cells even with an applied bias. Additional possible enhancements are proposed.

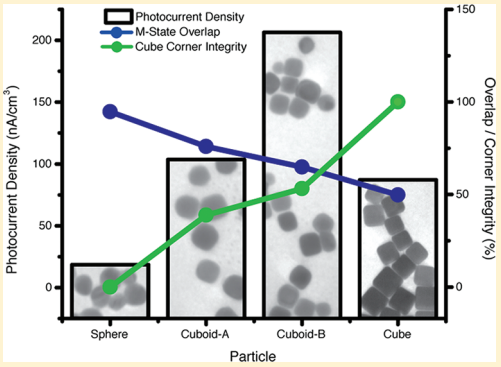

KEYWORDS: Bacteriorhodopsin, blue light effect, Nafion, nanoparticle, photocurrent, plasmonic enhancement

Bacteriorhodopsin (bR), the other natural photosynthetic system, is the light transducing membrane protein usually found in two-dimensional crystalline patches (purple membrane, PM) of *Halobacterium halobium*.[1−3] These patches make up the PM, which is composed of mainly protein (75% by wt.) and lipid (~25%).[4−6] The lattice parameters of crystallized PM have been investigated extensively, showing bR to be composed of seven helices with one interior retinal chromophore in a two-dimensional hexagonal structure.[1−6] This light-driven proton pump moves protons from the cytoplasmic to the extracellular side of its membrane.[7] Under continuous wavelength (cw) illumination, bR exhibits a stationary photocurrent as it transforms light energy into electrochemical energy in the form of a proton gradient across its membrane.[8−10] It offers advantages for its ease of generation and handling, as well as for its durability over a wide range of temperature,[11] pH,[12] and salt concentration ranges.[11,12] These unique characteristics make bR promising for applications in solar energy; however, a limitation arises from its relatively poor native solar energy conversion efficiency[10] compared to other materials, such as semiconducting metal oxides.[13] Indeed, the photocurrent density values reported so far in bR thin film systems are only 0.2−40 pA cm^{-2} per monolayer even with the use of an applied bias.[14]

Recently, our group constructed a solution-based electrochemical cell that has no need for an external bias and does not require bR film preparation.[15] This cell, constructed from ITO glass and a molecular porous membrane, generated a bR photocurrent as high as 1.5 nA/cm^3.[15] In an effort to enhance the photocurrent generation of bR, we exploited the surface plasmon effect. Surface plasmon resonance is induced by coupling of the incident electromagnetic light wave with the conduction band electrons in a metal nanoparticle. Silver nanoparticles, in particular, have a plasmon resonance band that overlaps well with the M intermediate absorption in the blue wavelength region and should enable us to intensify what is known as the blue light effect.[16,17] The blue light effect occurs when the M intermediate of the photocycle absorbs a blue photon (350−550 nm), resulting in rapid reprotonation and chromophore reisomerization back to the bR ground state in hundreds of nanoseconds (Figure 1).[17,18] Under normal thermal conditions, the photocycle progresses through a series of slow conformational changes and requires 15 ms for the M intermediate to be converted back to the bR ground state.[19,20] Thus, in speeding up the proton pumping process, the blue light effect greatly enhances photocurrent generation.

Received: June 3, 2011
Revised: July 26, 2011
Published: July 29, 2011

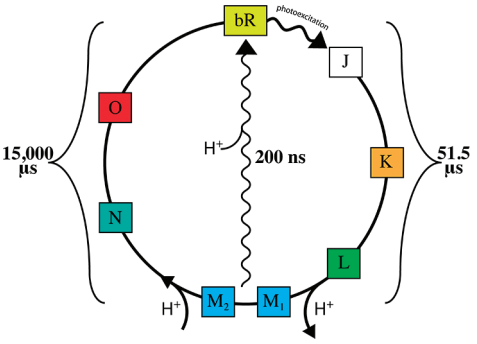

Figure 1. Simplified bR photocycle. The photocycle is initiated upon the absorption of light by the retinal chromophore. The formation of M is associated with the loss of a proton to the exterior of the membrane, while the formation of N involves reprotonation of the system by a proton inside the membrane. As a result, a proton gradient is created across the membrane. The M intermediate either can thermally relax to the bR ground state through a series of conformational changes in a time of 15 ms,or can be photochemically converted back to the bR ground state in a time of 200 ns via absorption of blue light. The color of the box around each intermediate reflects its spectral absorbance wavelength in the visible region.

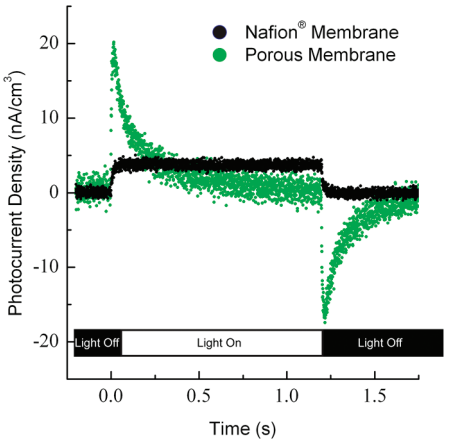

Figure 2. Bacteriorhodopsin native photocurrent generation using porous (green) and Nafion (black) membranes. The steady state current is enhanced as a result of the proton selectivity of the Nafion membrane.

We found that the bR photocurrent is greatly enhanced in the presence of silver nanoparticles when the electrochemical cell is exposed to blue light.[16] The plasmonic field of silver nanoparticles greatly enhances the flux of blue photons, leading to an enhancement of the blue light effect and to a consequent increase in the rate of proton release. This results in an enhanced steady-state proton concentration and photocurrent. The maximum photocurrent we have previously reported is 25 nA/cm^3, using bR mixed with silver nanoparticles (1.2 nM) capped with citrate molecules.[16]

To make bR more promising for solar energy applications, we must maximize the photocurrent generation, which requires maximization of each of three enhancement components. (1) Maximize the proton polarization in the solution cell. The nonselective porous membrane is substituted for a proton-selective Nafion membrane. (2) Minimize screening of surface field intensity by optimizing the capping material thickness around the nanoparticle. The charged nature of the Nafion membrane precludes the use of capping agents such as citrate. The most favorable molecular weight of a neutral polymer capping agent (PVP) was chosen based on maximum photocurrent enhancement and best stability. (3) Maximize the plasmonic field intensity and spectral overlap with the M intermediate to maximize the blue light effect. Silver nanocubes and cuboids were used to find the maximum photocurrent enhancement by exploring the trade-off between the very high field intensities associated with cube shapes and the good spectral overlap of more rounded shapes. Using the Nafion membrane and the 40 nm silver cuboid nanoparticle capped with 55k molecular weight PVP polymer, we report a maximum photocurrent of 0.2 μA/cm^3, which is 5000 times larger than published results for thin film bR electrochemical cells.

Minimizing Ionic Depolarization Effects in the bR Electrochemical Solution Cell. A porous membrane was used in our previous bR electrochemical cell to separate the two half-cells (bR working cell and reference cell).[16] Porous membranes are attractive for their low cost, but they suffer from nonselective transport of cations and anions across the membrane.[21] This leads to an initial spike in the photocurrent density that results from rapid proton flux across the membrane, and it is followed by a decay in photocurrent density as the larger, bulkier anions traverse the membrane and begin neutralizing some of the charges (Figure 2). This porous membrane generated a stationary photocurrent of 1.5 nA/cm^3, which is only 7% of the intensity of the initially formed photocurrent (20 nA/cm^3).

Known for their ability to generate stable photocurrents, Nafion membranes have come into widespread use for applications in areas such as proton exchange membrane (PEM) fuel cells.[22] These membranes exhibit selectivity for cations through the use of anionic channels and thereby limit the flux of anions across the membrane.[23] This increases the overall charge carrier separation and allows for a stable photocurrent (4.6 nA/cm^3) that is higher than that generated by the porous membrane. Figure 2 illustrates this gain in the steady state current. However, it also shows that we did not reach the initial polarization seen in the transient spike with the porous membrane. This might suggest that by finding a more efficient cation-selective membrane, we might get a great deal more current enhancement.

Minimizing Shielding of the Surface Plasmon Fields. The previously used citrate-capped silver nanoparticles are not suitable for this work, as the charged nature of the Nafion membrane destabilizes charged capping agents and leads to particle aggregation. We instead tried several different molecular weights of poly(vinylpyrrolidone) (PVP) polymers in order to select the polymer providing the best stability with the thinnest capping shell, as shell thickness screens the nanoparticle surface field felt by the bR molecules in solution. We studied both the plasmonic field enhancement of the bR photocurrent and the stability of the silver nanoparticles as a function of capping shell thickness. The silver nanospheres with varied chain-length PVP capping agent were prepared via a polyol process[24] using PVP polymers of 10000, 55000, and 365000 g/mol molecular weight in separate syntheses (procedure and instrumentation in the Supporting Information). The synthesized silver spherical nanoparticles of roughly 40 nm ($\pm$5 nm) diameter showed excellent spectral overlap with the M intermediate absorption in bR (Figure 3A). The dynamic light scattering (DLS) technique was used to measure the hydrodynamic diameter of the resulting particles, and transmission electron microscopy (TEM) was used to measure the diameter of the metallic core. Since the particles

dx.doi.org/10.1021/nl2018959 |Nano Lett. 2011, 11, 3821–3826

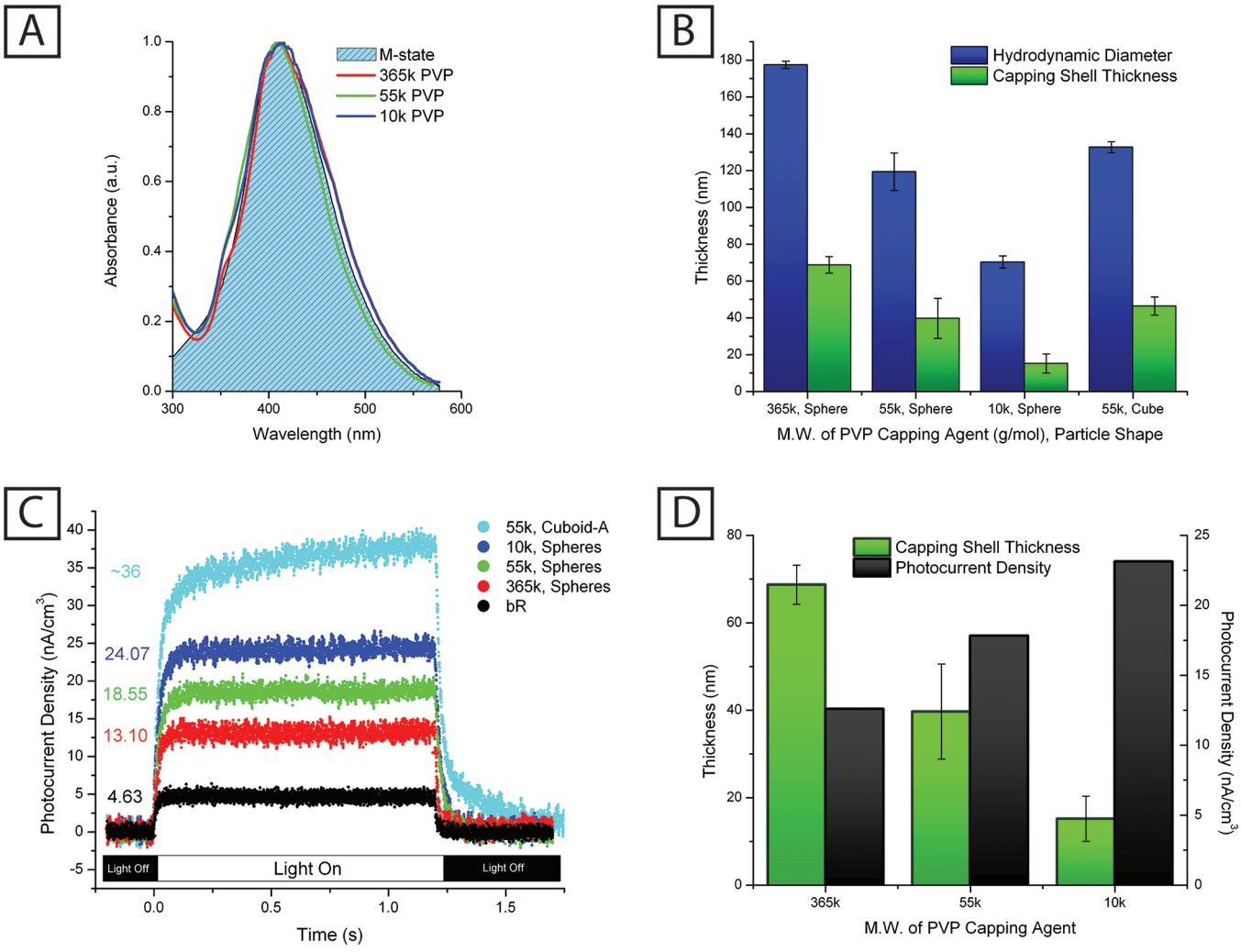

Figure 3. (A) Absorbance spectra of silver nanospheres capped with 10k (blue), 55k (green), and 365k (red) M.W. PVP showing spectral overlap with the M intermediate of bR (shaded cyan). (B) Hydrodynamic diameter (blue) and relative capping shell thickness (green) for 10k, 55k, and 365k M.W. PVP-capped silver spheres and 55k M.W. PVP-capped silver cubes. (C) Bacteriorhodopsin native photocurrent generation (black), bR photocurrent generation under enhancement by 40 nm silver spheres capped with PVP of MW 10k (blue), 55k (green), and 365k (red) and initial, short-time scale observation of enhancement using 40 nm edge length silver cuboid-A capped with 55k MW PVP (cyan). (D) Capping shell thickness (green) and bR photocurrent density (black) for silver spheres capped with PVP of the designated molecular weight. This inverse relationship results from the capping material shielding the particle plasmonic field.

have the same capping material, subtraction of the core radii from the hydrodynamic radii provides the relative capping shell thicknesses (Figure 3B). The full length of the smallest molecular weight PVP is approximately 600 nm, which is much larger than the thickness of the corresponding capping shell (18 nm). This suggests that the PVP is wrapped around the nanoparticles in a complex manner. Error bars on the hydrodynamic diameter represent the standard deviation among the 20 DLS measurements for each sample, and error bars on the capping shell thicknesses are propagated from both the hydrodynamic diameter measurements and the TEM measurements.

The photocurrent density of silver nanoparticles capped with different molecular weights of PVP was measured as follows. Bacteriorhodopsin, citrate buffer, and silver nanoparticles were mixed and covered with a Nafion membrane to serve as the bR working cell. On the other side of the membrane, citrate buffer solution served as the reference cell. The citrate buffer maintains the pH of both cells at 7.0 and provides for enhanced charge carrier separation. The photocurrent measurements were carried out under continuous wavelength white light with an external shutter and a signal amplifier. Dark incident photocurrent was collected before the addition of bR to eliminate any photoartifacts. This dark photocurrent density (0.8 nA/cm^3) was subtracted from the induced photocurrent values for bR reported herein.

Figure 3C (black) shows the photocurrent generation of a solution of bR and of bR/silver nanoparticle mixtures. During the irradiation period, the photocurrent reached a maximum steady state in about 50 ms and retained this maximum for the duration of the irradiation period. This plateau feature in the photocurrent profile and lack of spiking are a result of the proton selectivity of the Nafion membrane. Photocurrent measurements of bR in the presence of equivalent concentrations (2 nM) of each of our silver nanoparticles in turn showed an enhancement of the photocurrent with decreasing capping shell thickness (Figure 3C, red, green, blue). Stronger effective field intensity

dx.doi.org/10.1021/nl2018959 |*Nano Lett.* 2011, 11, 3821–3826

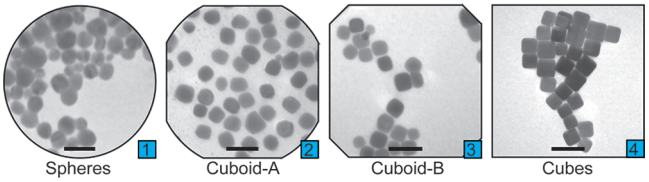

Figure 4. TEM images of spheres (1), cuboid-A with highly truncated corners (2), cuboid-B with slightly truncated corners (3), and perfect cubes (4) with shape-representative image frames. (Scale bars = 100 nm.)

from thinner capping shells yields larger photocurrent enhancement for these particles with virtually the same spectral overlap with the M intermediate (Figure 3A). This relationship between photocurrent generation and capping shell thickness is shown in Figure 3D.

Field strength is as critical as postulated, and the 10k PVP-capped spheres provided the best enhancement of the photocurrent; however, particle instability was noted spectrally and via TEM after several 10 min experiments with the same 10k PVP-capped particles. In contrast, the 55k- and 365k-capped particles showed stability up to at least 1 week in the presence of the reaction mixture of bR and citrate buffer, suggesting 55k PVP-capped particles to be the most attractive choice for their balance of large photocurrent enhancement and good long-term stability.

Particle Shape Effects: Spectral Overlap and Surface Field Enhancement. Since the 55k MW PVP provides for the best particle stability with the least detriment to plasmonic field strength, we used this capping agent in our efforts to study the shape dependence of silver nanoparticles on photocurrent enhancement. The unique surface plasmon resonance of metal nanoparticles is highly sensitive to their local environment as well as their size, shape, and composition.[25,26] Our previous work focused solely on spherical silver nanospheres, as their surface plasmon resonance spectrum has the best overlap with M intermediate absorption. Changing the shape of the particle to increase the field intensity should increase the photocurrent enhancement. However, altering particle shape also shifts the absorbance profile, thereby altering spectral overlap with the M intermediate. We examined a progression of shapes from spheres to cubes, all capped with 55k PVP and having very similar capping shell thicknesses (Figure 3A), in order to find the particle with both the strongest field and the best spectral overlap of the plasmon with the M intermediate absorption. Figure 4 shows the TEM images of these particles, which are referred to herein as perfect cubes, cubes with slightly truncated corners (cuboid-B), cubes with highly truncated corners (cuboid-A), and cubes with fully truncated corners (spheres). All crystalline nanoparticles (spheres, cubes, and cuboids) were synthesized using the same chemicals, reaction vessels, heat settings, capping agents, and cleaning techniques to ensure that particle and medium composition were consistent throughout. Shape variations were achieved by altering solution perturbation speed during synthesis, with slow stirring (~300 rpm) yielding cubes, high stirring (~900 rpm) generating spheres, and intermediate stirring (~450, ~550 rpm) yielding cuboids.

Metal nanoparticles with features such as corners and edges (e.g., prisms, cubes) are known to exhibit larger plasmonic field intensities than particles lacking these geometric features (spheres). We performed discrete dipole approximation (DDA) calculations[27,28] for a 40 nm silver sphere and a 40 nm edge length cube (Figure 5A). When shown on the same field intensity scale, cubes show the expected strongest field intensity at their edges and corners.

This increased field intensity is advantageous for the enhancement of bR photocurrent; however, a red shift in the plasmon resonance occurs as one progresses from a spherical shape to a cubic shape through cuboidal intermediates. In this progression from a spherical shape to a perfect cube, we see both increasingly better resolution of the cubic peaks and a gradual red shift in the plasmonic peak (Figure 5B) that results in less spectral overlap of the plasmon with the M intermediate absorption. We used this shape progression to study the trade-off between an increase in the plasmonic field strength and the decrease that ensues in the degree of spectral overlap with the M intermediate absorption.

Over the 1.2 s time scale (Figure 3C), the photocurrent density of bR in the presence of silver cuboid-B is much higher than even that of silver spheres capped with 10k MW PVP. However, the photocurrent density of cuboid-B over this 1.2 s exposure time was not stationary, showing a steady rise. The time scale was adjusted to 1000 s to investigate this. Over the course of this longer time scale experiment (Figure 5C), the bR photocurrent density remained the same for both the native bR and for the 55k MW PVP-capped silver spheres as that seen in the short time scale experiments (Figure 3C). However, for both cuboids and cubes, the photocurrent density increased dramatically, reaching a maximum after 100 s that was maintained over the course of the 1000 s exposure interval with no change in solution temperature (±0.1 °C). Cuboid-A, with highly rounded corners, reached a maximum of 103.6 nA/cm^3 after 100 s, a stark contrast to the ~36 nA/cm^3 photocurrent density observed over the 1.2 s time scale experiments. The highest photocurrent density achieved in these experiments utilized cuboid-B to produce a photocurrent of 0.2 μA/cm^3. This value is 50 times higher than pure bR in our wet electrochemical system (4.64 nA/cm^3) and 8 times higher than our previous report using silver nanospheres and a porous membrane system (25 nA/cm^3).[16] The large enhancement intensity results from the much stronger field associated with cuboid shapes compared to spheres, though the mechanism of the slower rise in photocurrent density is yet to be elucidated.

Interestingly, despite their even stronger field intensity, perfect cubes displayed less enhancement of the bR photocurrent than did cuboid-B. The absorption profile of these silver nanoparticles (Figure 5B) explains the reason why. The degree of spectral overlap with the M intermediate, which is necessary for the blue light effect to occur, decreases significantly as the shape changes from cuboid-B to perfect cubes. As we have shown previously, the higher degree of spectral overlap between the plasmonic particle and the M absorption results in a higher photocurrent density. These results and contributing factors are rendered visually in Figure 5D, where the peak in photocurrent density (black) is apparent for the particle that falls nearest the intersection of the plots of field strength (corner integrity, green) and spectral overlap with the M intermediate (blue). The highest photocurrent density of silver cuboid-enhanced bR is as high as 0.2 μA/cm^3, which is 10 times higher than that of bR enhanced by silver nanospheres (around 20 nA/cm^3) and orders of magnitude higher than published results. This high photocurrent density was found to be stable for up to 6 consecutive hours of continuous irradiation, demonstrating

dx.doi.org/10.1021/nl2018959 |*Nano Lett.* 2011, 11, 3821–3826

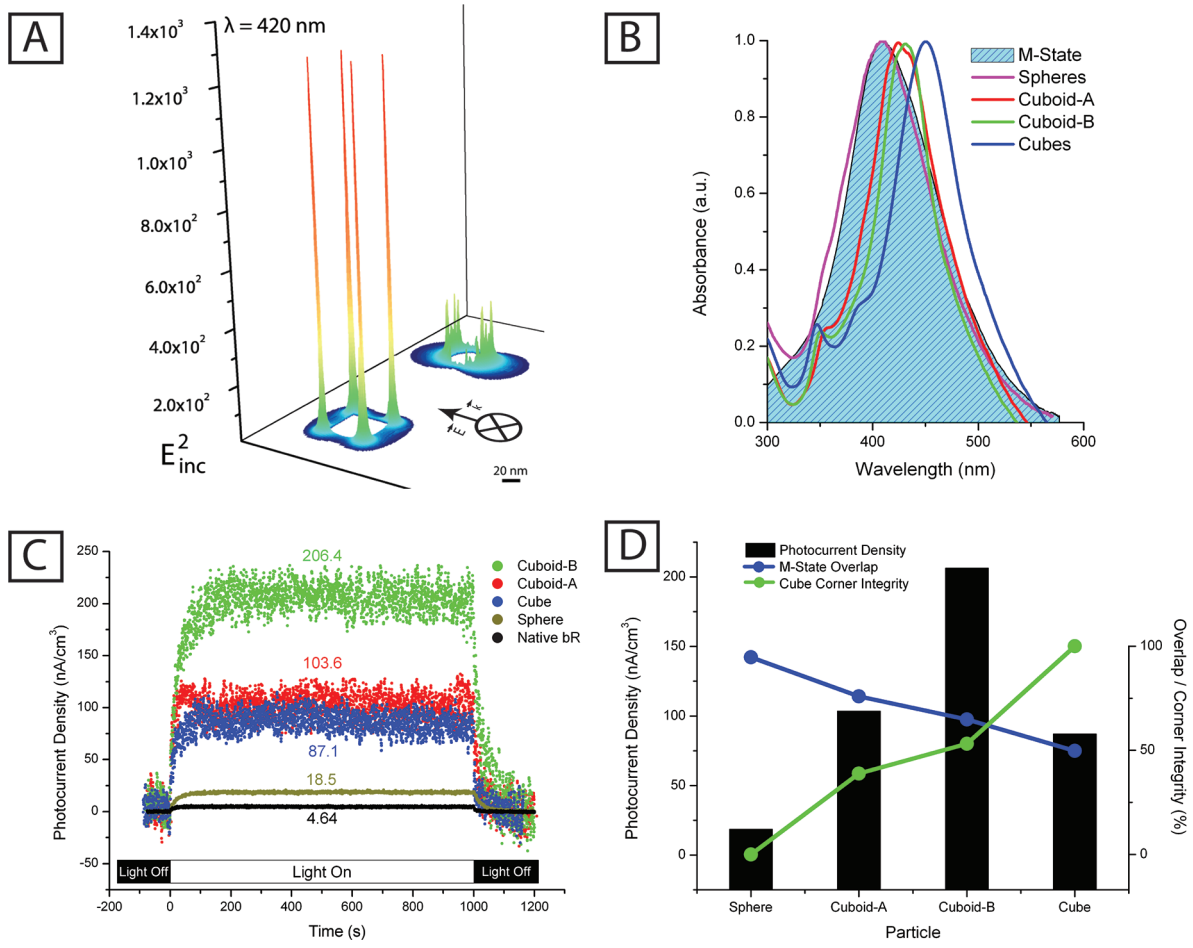

Figure 5. (A) Discrete dipole approximation plots of the three-dimensional electric fields for a 40 nm silver sphere (right) and a 40 nm edge length silver cube (left), demonstrating stronger plasmon field with sharper corners. (B) Absorbance spectra of 40 nm silver spheres, cuboids, and cubes capped with 55k MW PVP showing decreasing spectral overlap with the M intermediate of bR (shaded cyan) with increasing sharpness of cube corners. (C) Bacteriorhodopsin photocurrent generation under blue light enhancement from 40 nm silver particles capped with 55k MW PVP. Illustrates photocurrent enhancement of native bR (black) using spheres (yellow), cuboid-A with highly truncated corners (red), cuboid-B with slightly truncated corners (green), and perfect cubes (blue). (D) Photocurrent density of bR for each shape (black bars), spectral overlap between the surface plasmon resonance band of the nanoparticle and the M intermediate absorption (blue), and the cube corner integrity (green) as an indicator of field strength. Relative overlap percentage was determined via integration of the normalized curves, and relative corner integrity was measured using the radius of curvature from TEM images (full explanation in Supporting Information). This figure illustrates that the largest enhancement in photocurrent density results from the particle that falls nearest the intersection of spectral overlap and field strength, the 40 nm cuboid-B capped with 55k MW PVP.

the utility of specifically tailoring surface plasmons to the task at hand.

By making use of our knowledge of plasmonics, we were able to greatly enhance the photocurrent of the bacteriorhodopsin system. We first replaced the traditional thin film system, which can trap charge carriers, with a solution-based cell that requires no bias. We then used a cation-selective membrane to increase the proton polarization, demonstrating the need for highly selective membranes for maximum current enhancement. This work illustrates the need for both maximum particle field strength and plasmonic spectral overlap with the blue-light-absorbing M intermediate in plasmonic-enhanced bR electrochemical cells. The number of plasmonic nanoparticles with different field strengths and plasmon wavelengths is increasing with time. Finding a new particle that has a stronger electromagnetic field, better spectral overlap with the M intermediate, and a small capping shell is quite possible and will lead to maximum photocurrent enhancement.

■ ASSOCIATED CONTENT

Ⓢ Supporting Information. Details of preparation and procedures. This material is available free of charge via the Internet at http://pubs.acs.org.

■ AUTHOR INFORMATION

Corresponding Author

*E-mail: melsayed@gatech.edu.

Author Contributions

†These authors contributed equally to this work.

■ ACKNOWLEDGMENT

The authors would like to thank the DOE for financial support from Grant No. DE-FG02-97-ER 14799. Also, much gratitude to Lauren Austin and the lab of Dr. Nils Kröger for help with the DLS measurements, Brian Snyder for assistance with TEM,

Dr. Nageh Allam for constructive input, and Adam Poncheri for feedback and editing.

REFERENCES

(1) Oesterhe., D; Stoecken., W *Nat. New Biol.* **1971**, *233*, 149.
(2) PebayPeyroula, E.; Rummel, G.; Rosenbusch, J. P.; Landau, E. M. *Science* **1997**, *277*, 1676.
(3) Essen, L. O.; Siegert, R.; Lehmann, W. D.; Oesterhelt, D. *Proc. Natl. Acad. Sci. U.S.A.* **1998**, *95*, 11673.
(4) Luecke, H.; Richter, H. T.; Lanyi, J. K. *Science* **1998**, *280*, 1934.
(5) Luecke, H.; Schobert, B.; Richter, H. T.; Cartailler, J. P.; Lanyi, J. K. *J. Mol. Biol.* **1999**, *291*, 899.
(6) Edman, K.; Nollert, P.; Royant, A.; Belrhali, H.; Pebay-Peyroula, E.; Hajdu, J.; Neutze, R.; Landau, E. M. *Nature* **1999**, *401*, 822.
(7) Mitchell, P. *Nature* **1961**, *191*, 144.
(8) Chu, L. K.; Yen, C. W.; El-Sayed, M. A. *J. Phys. Chem. C* **2010**, *114*, 15358.
(9) Horn, C.; Steinem, C. *Biophys. J.* **2005**, *89*, 1046.
(10) Walter, J. M.; Greenfield, D.; Liphardt, J. *Curr. Opin. Biotechnol.* **2010**, *21*, 265.
(11) Vogel, R.; Siebert, F. *Biochemistry* **2002**, *41*, 3536.
(12) Zimanyi, L.; Varo, G.; Chang, M.; Ni, B. F.; Needleman, R.; Lanyi, J. K. *Biochemistry* **1992**, *31*, 8535.
(13) Hayden, S. C.; Allam, N. K.; El-Sayed, M. A. *J. Am. Chem. Soc.* **2010**, *132*, 14406.
(14) Jin, Y. D.; Honig, T.; Ron, I.; Friedman, N.; Sheves, M.; Cahen, D. *Chem. Soc. Rev.* **2008**, *37*, 2422.
(15) Chu, L. K.; Yen, C. W.; El-Sayed, M. A. *Biosens. Bioelectron.* **2010**, *26*, 620.
(16) Yen, C. W.; Chu, L. K.; El-Sayed, M. A. *J. Am. Chem. Soc.* **2010**, *132*, 7250.
(17) Hessling, B.; Herbst, J.; Rammelsberg, R.; Gerwert, K. *Biophys. J.* **1997**, *73*, 2071.
(18) Neutze, R.; Pebay-Peyroula, E.; Edman, K.; Royant, A.; Navarro, J.; Landau, E. M. *Biochim. Biophys. Acta, Biomembr.* **2002**, *1565*, 144.
(19) Ormos, P.; Dancshazy, Z.; Karvaly, B. *Biochim. Biophys. Acta* **1978**, *503*, 304.
(20) Kuhlbrandt, W. *Nature* **2000**, *406*, 569.
(21) Granick, S. *Science* **1991**, *253*, 1374.
(22) Oetjen, H. F.; Schmidt, V. M.; Stimming, U.; Trila, F. *J. Electrochem. Soc.* **1996**, *143*, 3838.
(23) Zawodzinski, T. A.; Derouin, C.; Radzinski, S.; Sherman, R. J.; Smith, V. T.; Springer, T. E.; Gottesfeld, S. *J. Electrochem. Soc.* **1993**, *140*, 1041.
(24) Sun, Y. G.; Xia, Y. N. *Science* **2002**, *298*, 2176.
(25) Kelly, K. L.; Coronado, E.; Zhao, L. L.; Schatz, G. C. *J. Phys. Chem. B* **2003**, *107*, 668.
(26) Daniel, M. C.; Astruc, D. *Chem. Rev.* **2004**, *104*, 293.
(27) Draine, B. T.; Flatau, P. J. *J. Opt. Soc. Am. A* **1994**, *11*, 1491.
(28) Draine, B. T.; Flatau, P. J. Scripps Institution of Oceanography, University of California: San Diego, CA, 2005.